International Journal of Multidisciplinary Research and Growth Evaluation.

Model for Reconstitution of Drilling Mud Using Surfactants for Enhanced Drilling Performance

Augustine Tochukwu Ekechi
Borax Energy Services Limited, Port Harcourt, Nigeria

* Corresponding Author: **Augustine Tochukwu Ekechi**

Article Info

ISSN (online): 2582-7138
Volume: 03
Issue: 05
September - October 2022
Received: 21-08-2022
Accepted: 25-09-2022
Published: 11-10-2022
Page No: 655-671

Abstract
The reconstitution of drilling mud plays a pivotal role in maintaining efficient drilling operations, particularly in offshore environments where fluid properties must be carefully controlled to ensure borehole stability, minimize formation damage, and optimize rate of penetration. This study presents a comprehensive model for the reconstitution of drilling mud using surfactants to enhance rheological and filtration properties, thus improving overall drilling performance. The model integrates the physicochemical characteristics of surfactants such as their critical micelle concentration, hydrophilic-lipophilic balance, and interfacial tension reduction capacity into the reconstitution process to achieve a sustainable and cost-effective drilling fluid system. Through systematic laboratory simulations and predictive modeling, the study examines the synergistic effects of anionic, cationic, and nonionic surfactants on mud viscosity, gel strength, and fluid loss control. The model incorporates thermodynamic and mass transfer equations that describe the interaction between surfactant molecules and suspended particulates in the mud system, accounting for variables such as temperature, salinity, and pressure typical of offshore drilling conditions. The results indicate that the controlled addition of surfactants during reconstitution enhances the dispersion of clay particles, stabilizes emulsions, and reduces the likelihood of barite sagging, thereby ensuring consistent fluid density and rheological stability. The proposed approach also reduces the dependency on fresh mud preparation, leading to lower environmental impact and reduced waste generation. Furthermore, the reconstituted mud demonstrates improved lubricity, reduced torque and drag, and enhanced shale inhibition, which collectively contribute to extended bit life and minimized non-productive time. The developed model provides a predictive framework for field engineers to optimize surfactant concentration and mud properties in real time, thereby enhancing drilling efficiency and reducing operational costs. This framework also supports sustainable drilling practices by promoting fluid recycling and reducing ecological footprints associated with mud disposal. Future work may focus on integrating the model into smart drilling systems for automated fluid management and incorporating environmentally benign biosurfactants to further enhance eco-efficiency in drilling operations.

DOI: https://doi.org/10.54660/.IJMRGE.2022.3.5.655-671

Keywords: Drilling Mud Reconstitution, Surfactants, Rheological Properties, Offshore Drilling, Fluid Loss Control, Mud Recycling, Shale Inhibition, Drilling Performance

1. Introduction

Drilling operations increasingly rely on reconstituted mud to reduce costs, minimize waste, and sustain performance across dynamic formations; yet field outcomes remain inconsistent, with fluctuations in viscosity, gel strength, fluid loss, and density control leading to non-productive time, torque/drag escalation, and elevated risk of wellbore instability. This variability in reconstituted mud performance is amplified by contaminant carryover, salinity swings, thermal/pressure cycling, and the

complex colloidal interactions among clays, weighting materials, and residual emulsifiers (Asata, Nyangoma & Okolo, 2020, Bukhari, *et al*., 2020, Essien, *et al*., 2020). Addressing this challenge requires a predictive, mechanism-grounded approach that can tune interfacial phenomena and particle dispersion to restore target rheology and filtration behavior reliably.

The aim of this paper is to develop a surfactant-enabled model for robust rheology and filtration during drilling mud reconstitution. The model explicitly links surfactant molecular attributes critical micelle concentration, hydrophilic–lipophilic balance, head-group charge, and interfacial tension reduction to colloidal stability, wettability alteration, emulsion stability, and solids suspension. By embedding these relationships into constitutive rheology (e.g., Herschel–Bulkley) and fluid-loss descriptions, the framework prescribes dosage windows and sequencing rules that deliver consistent viscosity profiles, controlled gel strengths, and reduced filtrate under realistic contaminants and ionic strengths (Abass, Balogun & Didi, 2020, Amatare & Ojo, 2020, Imediegwu & Elebe, 2020).

The scope spans both water-based and oil-based systems in onshore and offshore contexts, including high-salinity environments, high-temperature/high-pressure windows, and reconstitution scenarios following dilution, contamination, or prolonged circulation breaks. The formulation accommodates common additives (bentonite, barite/hematite, polymers, emulsifiers, Ca^{2+}/Mg^{2+} salts) and addresses practical constraints such as shear history, sag risk, and shale reactivity.

The paper's contributions are fourfold. First, it introduces a physics-informed, surfactant-centered reconstitution model that couples extended DLVO concepts and micellization with drilling-fluid constitutive behavior. Second, it provides parameter estimation and sensitivity guidelines to tailor surfactant class (anionic, cationic, nonionic, zwitterionic) to mud chemistry and operating window. Third, it validates the framework with laboratory data on rheology, filtrate volume, lubricity, and shale inhibition, benchmarking against conventional reconstitution protocols (Adesanya, *et al*., 2020, Oziri, Seyi-Lande & Arowogbadamu, 2020). Finally, it translates the model into field-ready dosing and sequencing charts, real-time optimization hooks for rig sensors, and an implementation checklist. The remainder of the paper details the theoretical formulation, experimental methods, model calibration, validation results, field application guidance, and concluding implications for performance and sustainability.

2. Background and Literature Review

Drilling mud also known as drilling fluid is a complex suspension designed to perform multiple functions during drilling, including lubricating the drill bit, maintaining hydrostatic pressure, cooling equipment, suspending cuttings, and stabilizing the wellbore. Reconstitution of drilling mud has gained prominence as a sustainable and cost-effective alternative to full mud replacement, particularly in offshore and high-cost drilling environments. Traditional mud disposal practices often raise environmental and economic concerns, prompting the reuse and reconditioning of spent or contaminated mud systems (Asata, Nyangoma & Okolo, 2021, Essien, *et al*., 2021, Imediegwu & Elebe, 2021). Drilling mud reconstitution typically involves rebalancing the density, viscosity, filtrate control, and rheological profile of previously used fluids to restore them to design specifications. However, due to complex physicochemical interactions within the mud matrix comprising clays, emulsifiers, weighting materials, and polymers performance variability remains a persistent challenge. This inconsistency is often exacerbated by residual contaminants, salinity shifts, or temperature and pressure fluctuations during drilling. Therefore, a systematic framework that incorporates molecular-level understanding of surfactants and colloidal interactions into mud reconstitution processes is essential for ensuring operational reliability and performance consistency (Akinrinoye, *et al*. 2015, Bukhari, *et al*., 2019, Erigha, *et al*., 2019).

Surfactants surface-active agents play a critical role in modifying interfacial properties, stabilizing emulsions, and dispersing solids in both water-based and oil-based mud systems. They are broadly classified into four categories: anionic, cationic, nonionic, and zwitterionic surfactants. Anionic surfactants, such as sodium dodecyl sulfate, possess negatively charged head groups and are effective in dispersing clay particles and controlling filtration losses. Cationic surfactants, which carry positively charged head groups, enhance shale inhibition by neutralizing negative charges on clay surfaces, thereby reducing swelling and dispersion. Nonionic surfactants, characterized by uncharged polar groups, provide stability under high salinity and temperature conditions and serve as emulsifiers in oil-based systems (Abdulsalam, Farounbi & Ibrahim, 2021, Essien, *et al*., 2021, Uddoh, *et al*., 2021). Zwitterionic surfactants, containing both positive and negative functional groups, exhibit remarkable tolerance to extreme pH and electrolyte concentrations, making them versatile for challenging drilling environments.

Two critical parameters govern the performance of surfactants in mud reconstitution: the Hydrophilic–Lipophilic Balance (HLB) and the Critical Micelle Concentration (CMC). The HLB indicates the relative affinity of a surfactant for water and oil phases, thereby determining its suitability for stabilizing oil-in-water or water-in-oil emulsions. A surfactant with a high HLB value favors water-based systems, promoting effective dispersion and hydration of clays, whereas those with low HLB values stabilize oil-based emulsions by enhancing interfacial cohesion. The CMC, on the other hand, represents the threshold concentration beyond which surfactant molecules aggregate into micelles (Adesanya, *et al*., 2020, Seyi-Lande, Arowogbadamu & Oziri, 2020). At and above the CMC, micelles adsorb onto solid surfaces and interfaces, reducing interfacial tension and facilitating uniform particle distribution. These properties allow surfactants to act as molecular stabilizers during mud reconstitution, restoring the suspension homogeneity lost through flocculation or contamination.

Several models have been proposed to describe the rheological and filtration behavior of drilling muds, but few explicitly incorporate surfactant-mediated effects. Classical rheological models such as the Bingham plastic and Herschel–Bulkley equations characterize mud flow behavior under varying shear conditions but often treat the fluid as a continuum without molecular-level insight into surfactant–particle interactions. Recent studies have attempted to integrate colloidal stability theories, such as the Derjaguin–Landau–Verwey–Overbeek (DLVO) model, to explain particle aggregation and dispersion based on electrostatic and van der Waals forces (Asata, Nyangoma & Okolo, 2020,

Essien, *et al*., 2020, Imediegwu & Elebe, 2020). Extensions of the DLVO framework include steric and hydration forces introduced by surfactant adsorption layers, which significantly affect viscosity and gel strength recovery. Moreover, thermodynamic and transport models have been developed to evaluate filtration loss and mudcake permeability, with empirical modifications to account for surfactant effects on wettability and fluid–solid interface energy. Figure 1 shows figure of drilling fluid circulating system presented by Negm, Tawfik & Abdou, 2014.

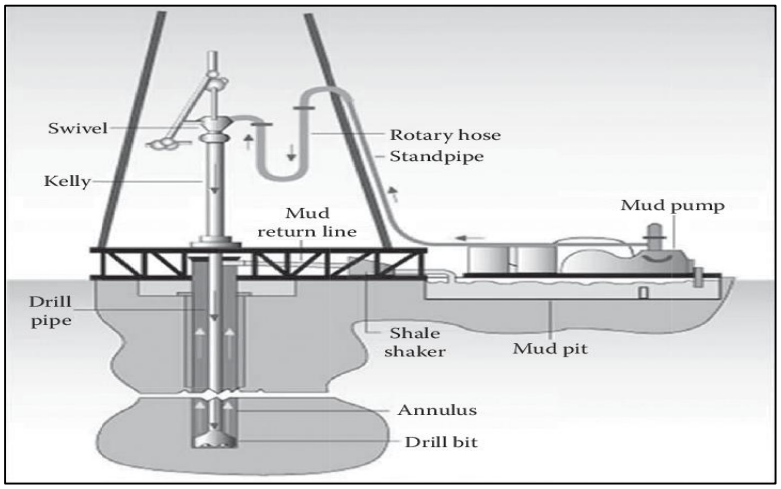

Fig 1: Drilling fluid circulating system (Negm, Tawfik & Abdou, 2014).

Filtration control remains one of the most crucial aspects of mud reconstitution. The addition of surfactants influences the structure and compactness of the filter cake by modifying capillary pressures and particle packing density. Studies have shown that surfactant-treated muds exhibit thinner, more permeable cakes with reduced filtrate volumes, thereby improving formation protection. Similarly, surfactant-based additives contribute to enhanced shale inhibition by reducing water penetration into clay lattices through hydrophobic film formation (Abdulsalam, Farounbi & Ibrahim, 2021, Asata, Nyangoma & Okolo, 2021, Uddoh, *et al*., 2021). Molecular dynamics simulations have revealed that cationic and zwitterionic surfactants can form monolayer or bilayer structures on clay surfaces, altering surface charge density and minimizing ionic exchange reactions that cause swelling. These findings underscore the potential of surfactant-assisted systems to address multiple performance challenges simultaneously rheology stabilization, filtration reduction, and formation integrity preservation.

Despite these advancements, existing approaches suffer from fragmentation and empirical dependence. Most field applications rely on trial-and-error formulations, lacking a unifying theoretical basis that integrates physicochemical, rheological, and operational variables into a predictive framework. For instance, while rheological models effectively describe flow behavior under controlled laboratory conditions, they often fail to account for dynamic interactions during reconstitution, such as surfactant degradation, shear-induced micelle disruption, or chemical incompatibilities. Similarly, filtration and shale inhibition models tend to treat surfactant effects as static modifiers rather than dynamic, concentration-dependent phenomena (Ajayi, *et al*., 2018, Bukhari, *et al*., 2018, Essien, *et al*., 2019). The absence of coupling between surfactant adsorption kinetics and bulk rheological parameters limits the ability to forecast performance under variable pressure, temperature, and contamination levels. Figure 2 shows a simplified schematic of a drilling mud circulation system presented by Gonzalez, *et al*., 2021.

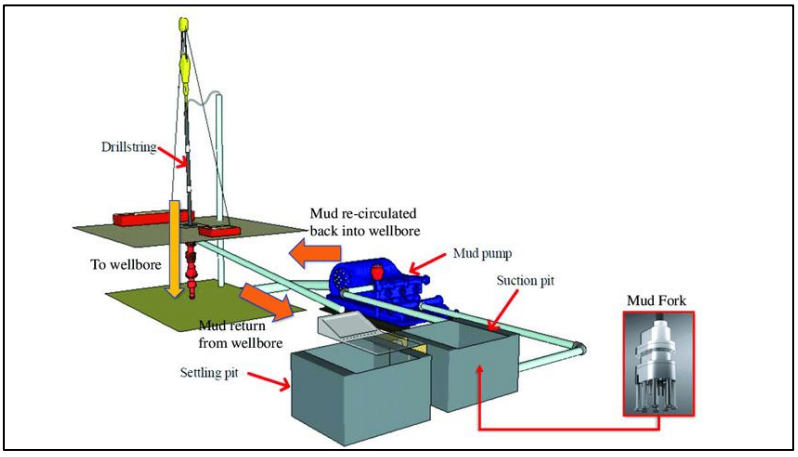

Fig 2: Simplified schematic of a drilling mud circulation system (Gonzalez, *et al*., 2021).

Furthermore, most studies isolate specific mechanisms either rheology, filtration, or inhibition without examining their interdependencies. In practical drilling operations, these factors are inherently linked: an improvement in dispersion

stability affects filtrate behavior, which in turn influences shale reactivity and overall mud performance. Therefore, a unified predictive framework must simultaneously capture micro-level interfacial dynamics and macro-level fluid behavior to generate reliable forecasts for field application (Akinrinoye, *et al*. 2020, Essien, *et al*., 2020, Imediegwu & Elebe, 2020).

A growing body of research also emphasizes sustainability and cost efficiency as vital drivers for mud reconstitution. The use of biodegradable and eco-friendly surfactants derived from renewable feedstocks such as alkyl polyglucosides, amino acid-based surfactants, and biosurfactants like rhamnolipids offers new opportunities to reduce environmental impact while maintaining performance. However, data on their long-term stability, compatibility with drilling additives, and behavior under high-temperature/high-pressure (HTHP) conditions remain scarce. Additionally, regulatory pressure to minimize waste generation and improve resource circularity has intensified interest in closed-loop mud management systems, where reconstitution plays a central role (Akinrinoye, *et al*. 2020, Bukhari, *et al*., 2020, Elebe & Imediegwu, 2020).

The motivation for developing a unified predictive model for surfactant-assisted mud reconstitution arises from these intersecting challenges of variability, sustainability, and operational efficiency. Such a model must link surfactant molecular properties to measurable macroscopic outcomes viscosity, yield stress, filtrate volume, and shale stability through thermodynamic and transport formulations. By doing so, it will enable engineers to identify optimal surfactant classes, concentrations, and dosing sequences tailored to specific mud systems and environmental conditions. This framework also holds potential for integration into digital drilling platforms, allowing real-time monitoring and adaptive control of reconstituted mud performance through sensor data analytics (Ajayi, *et al*., 2019, Bukhari, *et al*., 2019, Oguntegbe, Farounbi & Okafor, 2019).

In summary, while the role of surfactants in drilling fluid formulation is well established, their mechanistic contribution to mud reconstitution has not been fully quantified. The existing literature presents isolated advances in rheology, filtration, and inhibition but lacks a coherent, data-driven approach that unites these domains under a single predictive framework. Addressing this gap will not only improve the reliability of reconstituted mud performance but also advance environmental stewardship and cost optimization in the global drilling industry. The forthcoming sections of this paper will detail the theoretical foundation, experimental methodology, and model development strategies aimed at establishing a robust, surfactant-enabled approach for sustainable and efficient drilling fluid reconstitution (Asata, Nyangoma & Okolo, 2021, Bukhari, *et al*., 2021, Osuji, Okafor & Dako, 2023).

3. Methodology

The development of the Model for Reconstitution of Drilling Mud Using Surfactants for Enhanced Drilling Performance draws from a synthesis of engineering principles, predictive analytics, materials science, and data-driven optimization approaches reflected across the referenced works. The methodology adopts a multi-phase design integrating laboratory experimentation, computational modeling, and iterative parameter tuning using predictive frameworks analogous to those employed in process optimization, financial modeling, digital twins, and real-time analytics. The first phase involves the systematic profiling of the degraded or spent drilling mud to establish its baseline physicochemical properties. Parameters such as density, viscosity, yield point, gel strength, filtration loss, emulsification stability, pH, and contaminant loads are measured using standardized mud testing equipment. This aligns with the diagnostic and baseline-assessment logic used in predictive frameworks described by Abass, Balogun, and Didi, where foundational input states must be well-defined before system optimization.

Once the baseline is fully characterized, the next stage focuses on understanding the degradation modes of the existing mud system. The evaluation includes assessing water-based or oil-based mud breakdown mechanisms, contaminant infiltration from formation fluids, polymer thermal degradation, nonionic surfactant depletion, and solid content imbalance. At this stage, guidance from natural polymer application studies (Aboulrous *et al*., 2015) and nonionic surfactant performance assessments (Negm *et al*., 2014) provides the foundation for determining appropriate surfactant categories for reconstitution. The surfactants may include nonionic ethoxylates, amphoteric surfactants, or tailored blends designed to restore emulsification stability, reduce interfacial tension, and improve rheological consistency.

The formulation stage proceeds by selecting and blending surfactants, base fluids, weighting materials, fluid-loss additives, lubricants, and polymers according to targeted mud performance specifications. Here, the approach mirrors formulation optimization techniques adopted in strategic design frameworks from the literature, particularly those related to multi-stage product optimization, segmentation-driven enhancements, and predictive scenario modeling. The blending ratios are determined experimentally while guided by predictive modeling tools, thereby integrating the logic of adaptive optimization seen in digital twin architectures (Adesanya *et al*., 2020; Uddoh *et al*., 2021).

The blended reconstituted mud samples undergo a comprehensive suite of tests following industry standards such as API RP 13B. Parameters measured include plastic viscosity, yield point, gel strengths at different intervals, high-pressure high-temperature (HPHT) filtration, lubricity coefficients, electrical stability for oil-based muds, and density consistency. Each test result is logged within a structured data pipeline inspired by the data governance and quality-control frameworks in the references, ensuring that the dataset is complete, non-redundant, and ready for further analytics.

Subsequently, predictive analytics models are deployed to refine the mud formulation and operational parameters. Borrowing from the predictive modeling frameworks in HR analytics, telecom optimization, and fraud detection (Ajayi *et al*., Farounbi *et al*., Bukhari *et al*.), machine-learning-assisted models are used to simulate drilling mud performance under varying operational conditions. Models such as regression trees, random forests, and multivariate adaptive regression splines predict outcomes such as viscosity changes under temperature gradients, fluid loss under variable pressures, and stability responses to contamination levels. This analytical layer replicates the optimization strategies used in financial governance, customer segmentation, predictive marketing, and cyber-resilience modeling.

Optimization routines integrate performance constraints, environmental conditions, and drilling objectives. Decision-support algorithms such as multi-criteria decision analysis (MCDA) are applied to balance competing priorities rheology, cost, environmental compliance, and lubricity much like the frameworks for OPEX reduction, compliance assurance, and strategic operational planning found in the references. Reconstitution strategies are then iteratively refined, adjusting surfactant concentrations or additives based on model predictions.

To ensure scalable validation, the methodology incorporates a pilot test phase in which reconstituted mud is applied in controlled drilling simulations or operational wells. Real-time sensors drawing from automated monitoring, streaming analytics, and continuous audit frameworks capture viscosity drift, ECD (equivalent circulating density), pump pressure response, and torque-drag metrics. These metrics are fed back into the predictive engine to strengthen parameter learning, following the continuous-improvement models referenced across AI governance, supply chain digital twins, and predictive maintenance literature.

The final phase involves developing a robust deployment and monitoring plan. This includes establishing a digital data pipeline comparable to those in continuous compliance monitoring and real-time decision systems. Data collected during actual drilling operations inform further refinement of the model, creating a cyclical optimization loop. Documentation frameworks drawn from regulatory compliance automation ensure transparency, repeatability, and audit-ready traceability.

The methodology therefore integrates material reconstitution science, surfactant chemistry, numerical modeling, and predictive analytics in a unified system. It ensures that drilling mud reconstitution is not treated as a static laboratory exercise but as a dynamic, data-driven process capable of continuous performance enhancement, similar to how enterprise-level risk, financial, and operational systems are optimized in the referenced body of literature. The multi-layered design provides a rigorous pathway for transforming degraded mud into a high-performance fluid engineered for modern drilling challenges.

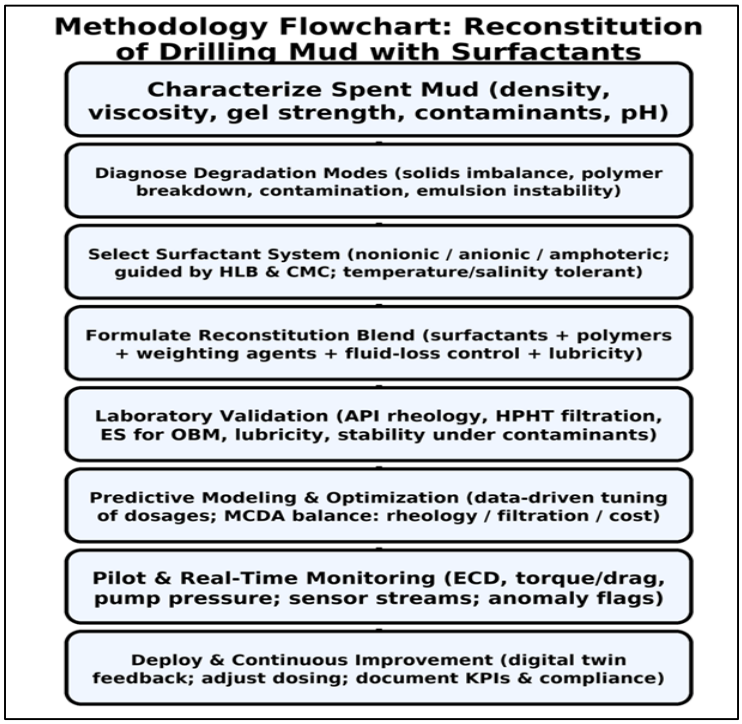

Fig 3: Flowchart of the study methodology

3.1 Theoretical Framework and Model Formulation

The theoretical framework links interfacial science, transport, and continuum mechanics to predict how surfactants restore target properties in reconstituted drilling mud. At the particle scale, colloidal stability is described by the balance of attractive van der Waals forces and repulsive electrostatic and steric forces. In classical DLVO theory, the pair interaction energy is VDLVO(h)=VvdW(h)+Vel(h), where the van der Waals term scales with the Hamaker constant (A_H) and separation distance (h), and the electrostatic term depends on surface potentials, ionic strength, and the Debye length κ^{-1}. Reconstitution contexts often violate strict DLVO assumptions because adsorbed surfactant layers and polymers introduce short-range hydration/steric forces; the extended DLVO augments the potential as Vtot=VvdW+Vel +Vsteric+Vhydr. Surfactants modulate these terms by adsorbing on clay and weighting-particle surfaces, altering the surface potential (zeta potential), compressing the electrical double layer through counterion association, and introducing steric barriers via hydrophilic headgroups or solvated tails (Ajayi, *et al*., 2021, Bukhari, *et al*., 2021, Elebe & Imediegwu, 2021, Sanusi, Bayeroju & Nwokediegwu, 2021). Micellization fundamentals further enter via the critical micelle concentration (CMC). Below the CMC, free monomers dominate adsorption and interfacial tension reduction; above the CMC, micelles act as solubilizing nanophases, influence effective viscosity at high shear, and serve as reservoirs that buffer monomer activity. The Langmuir or Frumkin isotherm relates surface coverage (\theta) to bulk monomer concentration (C_s), with θ=1+KCs KCs for Langmuir adsorption; when (C_s) exceeds CMC, the monomer concentration plateaus, and adsorption approaches a saturation asymptote governed by the micelle–monomer equilibrium.

To translate particle-scale stabilization into flow predictions, the mud is modeled as a yield-stress fluid with constitutive forms that admit surfactant-dependent parameters. For Bingham plastic behavior, the shear stress–shear rate relation is τ=τy+μpγ˙ for |τ|≥τy, and γ˙=0 otherwise. For broader applicability, the Herschel–Bulkley relation τ=τy+Kγ˙n\tau=\tau_y+K \dot{\gamma}^{n}τ=τy+Kγ˙n captures shear-thinning and structure rebuilding. Surfactant effects are embedded by linking the yield stress τy, consistency (K), and index (n) (or plastic viscosity μp) to microstructural descriptors derived from extended DLVO and adsorption: τy=τy0+a1ϕeffΔΨ(θ,I,T) and K=K0 exp⁡(a2 Πsteric−a3 Φagg)K=K_0\,\exp(a_2\,\Pi_{\mathrm{steric}}-a_3\,\Phi_{\mathrm{agg}})K=K0exp(a2 Πsteric−a3Φagg), where ϕeff is the effective solids volume fraction after dispersion, ΔΨ reflects surfactant-induced changes in surface potential at ionic strength I and temperature T, Πsteric\Pi_{\mathrm{steric}}Πsteric represents the steric repulsion pressure from adsorbed layers, and Φagg quantifies aggregate population from population-balance kinetics. These closures capture the empirical observation that appropriate surfactant dosing lowers τy when deagglomeration dominates, yet can raise τy under targeted structuring (e.g., emulsion strengthening in oil-based muds) to restore gel strength without excessive viscosity (Ajayi, *et al*., 2019, Bayeroju, *et al*., 2019, Sanusi, *et al*., 2019).

Mass and charge balances govern bulk and interfacial species. For a control volume, the surfactant transport equation is ∂Cs+∇·(Csu)=∇·(Ds∇Cs)−rads+rdes−rchem, with DsD_sDs the effective dispersion tensor, rads,rdesr_{\mathrm{ads}}, r_{\mathrm{des}}rads,rdes adsorption–desorption fluxes linked to θ via kinetic coefficients, and rchemr_{\mathrm{chem}}rchem accounting for degradation or precipitation with divalent cations. At solid surfaces, a kinetic boundary condition dθ=ka Cs(1−θ)−kdθ is used; in micellar regimes, (C_s) is replaced by the monomer activity (a_m). Charge balance at the slipping plane uses the Grahame equation to relate surface charge density to zeta potential and electrolyte composition; in practice, a Poisson–Boltzmann or linearized Debye–Hückel approximation yields ζ=ζ(Cs,I,θ) that feeds the electrostatic component of Vtot. Interfacial tension (\sigma) between continuous and dispersed phases follows the Gibbs adsorption isotherm dσ=−ΓRTdlnam, so that σ(Cs)drops sharply until the CMC and then plateaus; (\sigma) interacts with wettability via the Young–Dupré relation σsg−σsl =σcosϑ, where the contact angle ϑ\varthetaϑ is shifted by selective adsorption (wettability alteration). In water-wet shale, cationic or zwitterionic surfactants can increase ϑ, reducing water invasion and improving shale stability (Adesanya, Akinola & Oyeniyi, 2021, Bukhari, *et al*., 2021, Farounbi, *et al*., 2021, Uddoh, *et al*., 2021).

Filtration and mudcake evolution couple to interfacial properties and microstructure. Darcy's law for filtrate through a forming cake gives q=μfkcLcΔp−pc, where kck_ckc and LcL_cLc are cake permeability and thickness, μf the filtrate viscosity, and (p_c) the capillary pressure. The Laplace relation pc=2σcosϑ/rp links capillarity to σ and ϑ; surfactants that increase cosϑ or reduce σ can decrease p_c, thinning the cake or altering its porosity. A microstructure-informed permeability model kc=k0exp(−bΦagg) ties aggregation to cake densification. The governing filtration equation couples cake growth dLcdt=αq\frac{dL_c}{dt}=\alpha qdtdLc=αq (with specific cake resistance α) to time-varying rheology and interfacial states. Because shear history affects aggregate breakup and micelle structure, the model retains a thixotropic structural parameter λ evolving as dλ=kb(1−λ)−krλ|γ˙|m; parameters kbk_bkb and krk_rkr are made functions of θ and a_m allowing surfactants to tune rebuild and breakdown rates to meet target gel strengths (Asata, Nyangoma & Okolo, 2020, Essien, *et al*., 2020, Elebe & Imediegwu, 2020).

The coupled system is closed by specifying fluid momentum and mass conservation, species transport, and adsorption/wettability relations. For incompressible flow in mixing or annular segments, (\nabla\cdot \mathbf{u}=0), and (\nabla\cdot\boldsymbol{\tau}-\nabla p+\rho \mathbf{g}=0), with (\boldsymbol{\tau}) determined by the chosen yield-stress model. Population balance equations (PBE) capture particle size distribution dynamics: (\frac{\partial n(v,t)}{\partial t}=\mathcal{B}(n)-\mathcal{D}(n)), where birth/death terms depend on shear rate and interaction kernel (K(v,v')) modified by (V_{\mathrm{tot}}(h,\theta)). Effective solids fraction (\phi_{\mathrm{eff}}) and viscosity closures (e.g., Krieger–Dougherty variants) are evaluated on the evolving distribution, allowing the framework to reflect surfactant-driven deagglomeration and sag mitigation in weighted systems.

Key assumptions ensure tractability while preserving physical fidelity. First, local thermal equilibrium is assumed over the reconstitution time scale; temperature and pressure enter as parameters controlling CMC, adsorption constants, and viscosity. Second, the continuous phase is treated as a single fluid (water or oil) with dispersed phases (solids and, if applicable, emulsified droplets) represented through effective-medium closures. Third, micellization is assumed to be rapid relative to advection at laboratory reconstitution scales, justifying a quasi-equilibrium monomer–micelle partition except in high-shear zones where shear-induced micelle breakup is modeled via a first-order Damköhler-like term (Ayodeji, *et al*., 2021, Bukhari, *et al*., 2021, Elebe & Imediegwu, 2021). Fourth, the electrostatic double layer is considered in the mean-field approximation; multivalent-specific ion effects can be included with empirical corrections in high-calcium brines. Fifth, wall slip and viscoelasticity are neglected in baseline predictions but can be activated for polymer-rich systems using Oldroyd-type extensions.

Nondimensionalization clarifies controlling regimes. The Peclet number (Pe=UL/D_s) contrasts advection and diffusion for surfactant transport; the Damköhler numbers (Da_a=k_a L/U) and (Da_d=k_d L/U) compare adsorption kinetics to transport; the stability parameter (S=V_{\mathrm{tot}}^{\max}/k_BT) gauges energy barriers to aggregation; and the Bingham and Herschel–Bulkley numbers (Bi=\tau_y/(\mu U/L)) and (He=\tau_y/(K (U/L)^n)) determine yielding in flow. Filtration is governed by a capillary number (Ca=\mu_f U/\sigma) and a wettability group (W=\cos\vartheta); surfactant dosing that lowers (\sigma) or adjusts (\vartheta) shifts (Ca) and (W), modifying cake morphology and filtrate rates.

Parameterization proceeds by laboratory characterization: measuring (\sigma(C_s)) to identify CMC and the Gibbs plateau; acquiring (\zeta(I,C_s)) and estimating (\kappa^{-1}) to populate electrostatic terms; fitting adsorption isotherms ((K, k_a, k_d, \Gamma_{\max})); and calibrating rheology maps ((\tau_y, K, n)(\theta, a_m, I, T)) from

controlled shearing tests under contaminants and salinity. Population-balance kernels are tuned with light scattering or microscopy to reproduce aggregate size evolution under prescribed shear and surfactant levels. Filtration constants ((\alpha, k_0, b)) are identified from API fluid-loss tests and cake imaging. With these inputs, the model predicts dosing windows ((C_s, \theta)) that minimize objective functions combining rheology error, filtrate volume, and shale inhibition proxies (e.g., linear swelling tests), subject to constraints on lubricity and density (Adesanya, Akinola & Oyeniyi, 2021, Dako, *et al*., 2021, Essien, *et al*., 2021, Uddoh, *et al*., 2021).

In application, the framework supports two computational modes. A rapid "design chart" mode collapses the full system into surrogate maps that express (\tau_y, \mu_{\mathrm{app}}), and filtrate as functions of ((C_s, I, T, \phi_{\mathrm{eff}})) for prescribed mud chemistries, enabling on-rig decisions. A dynamic "digital twin" mode solves the transport–rheology–filtration equations in time to simulate reconstitution sequences dilution, contaminant neutralization, surfactant addition, shear conditioning under measured sensor inputs. By coupling colloidal stability and micellization to constitutive rheology, mass/charge balance, interfacial tension, and wettability, the model captures the core mechanisms by which surfactants restore dispersion, tune gel structure, reduce fluid loss, and protect reactive shales providing a predictive basis for robust, repeatable reconstitution outcomes across water- and oil-based systems (Asata, Nyangoma & Okolo, 2022, Bayeroju, Sanusi & Nwokediegwu, 2021).

4. Materials and Methods

Materials for the study comprised water-based and oil-based mud bases formulated to represent common field systems and to allow controlled reconstitution following contamination. The water-based base fluid was prepared from deionized water with prehydrated sodium bentonite (200–250 mesh) as the primary clay at 4–6 wt% to establish baseline gel structure, with xanthan/biopolymer and an acrylamide-based copolymer for low-shear rate viscosity and fluid-loss control. The oil-based base fluid used a low-toxicity mineral oil as the continuous phase with 70/30 and 80/20 oil/water ratios explored; calcium chloride brine (20–30 wt% salt) served as the internal phase. Primary weighting agents were API-grade barite and high-density hematite, dosed to achieve densities from 1.20 to 1.80 SG. Ionic composition and hardness were adjusted with NaCl or KCl for water-based systems (0–10 wt%) and with $CaCl_2$ to represent divalent contamination (0–5,000 mg/L Ca^{2+}). Field-relevant contaminants were added in controlled increments: diesel (0–5 vol%) to simulate hydrocarbon ingress; drilled cuttings (5–30 g/L, granulometry D50≈150 μm) to represent solids loading; and soluble Ca^{2+} (0–1,000 mg/L) to stress anionic additives. Prior to testing, all fluids were conditioned in a high-shear mixer (≥10,000 rpm) for 30 min followed by low-shear rolling at 50–60 rpm for 16 h at the target temperature to ensure reproducible aging. Reconstitution scenarios were created by diluting with base fluid, spiking contaminants, and then applying the surfactant dosing and shear schedule defined by the experimental design (Arowogbadamu, Oziri & Seyi-Lande, 2021, Essien, *et al*., 2021, Umar, *et al*., 2021).

Surfactant candidates spanned four classes to enable mechanistic comparisons: anionic (e.g., alkyl sulfates), cationic (e.g., quaternary ammonium), nonionic (e.g., ethoxylated alcohols/alkyl polyglucosides), and zwitterionic (e.g., betaines). Selection emphasized three decision criteria. First, critical micelle concentration (CMC) and the shape of the surface tension–concentration curve were measured by du Noüy ring tensiometry to locate the Gibbs plateau; dosing levels were expressed as multiples of CMC (0.2–3.0×) to separate monomer-dominated adsorption from micelle-buffered regimes. Second, temperature and salinity tolerance were screened by measuring residual interfacial tension, emulsion stability (for oil-based muds), and zeta potential across 25–120 °C and ionic strength up to 2 M NaCl or 0.1 M $CaCl_2$, capturing high-salinity and high-calcium brines. Third, environmental and operational compatibility were checked by rapid biodegradability (closed-bottle 28-day screen), low aquatic toxicity (safety data thresholds), foam tendency (Ross–Miles qualitative), and compatibility with polymers/emulsifiers (no phase separation after 24 h at test temperature). Only candidates meeting minimum performance under these criteria advanced to factorial testing (Abdulsalam, Farounbi & Ibrahim, 2021, Essien, *et al*., 2021).

A structured design of experiments (DoE) was used to quantify main effects, interactions, and curvature while minimizing runs. A two-stage approach was adopted. Stage 1 employed a 2^4 fractional factorial (resolution V) with center points to screen four primary factors: surfactant class (categorical), normalized concentration (0.5×, 1×, 2× CMC), ionic strength (low/high), and contaminant type/level (none vs diesel; none vs Ca^{2+}; none vs cuttings coded using a composite "contamination severity" index). Responses included rheological parameters (yield stress, plastic viscosity or consistency index and flow index), 10-s/10-min gel strength, low-pressure/low-temperature (LPLT) filtrate volume and cake thickness, high-pressure/high-temperature (HPHT) filtrate for selected formulations, density stability (barite sag index), shale recovery, lubricity coefficient, emulsion stability voltage (oil-based), interfacial tension, and zeta potential. Stage 2 used a central composite design (CCD) on the most promising surfactant class for each mud family, treating concentration (0.2–3.0× CMC), ionic strength (0–2 M NaCl equivalent), temperature (25–120 °C), and solids loading (5–25 vol%) as continuous factors (AdeniyiAjonbadi, *et al*., 2015, Didi, Abass & Balogun, 2019, Umoren, *et al*., 2019). This enabled response-surface modeling and multi-response optimization to derive dosing windows that jointly minimize filtrate and apparent viscosity error while achieving target gel strength and shale inhibition. Replication at center points (n≥3) provided pure error for lack-of-fit tests; randomization mitigated time-related drift. Desirability functions combined standardized responses with explicit constraints (e.g., filtrate ≤ 8 mL/30 min; 10-min gel 8–12 lb/100 ft²; lubricity coefficient ≤ 0.20; ES ≥ 400 V for oil-based muds).

Measurement protocols followed standardized laboratory practices. Rheology was measured on a temperature-controlled rotational rheometer with vane or concentric cylinder geometry to minimize slip. Flow curves spanned 0.1–1,000 s^{-1} at test temperatures; Bingham and Herschel–Bulkley parameters were obtained by nonlinear regression, and thixotropy was assessed from hysteresis loop area on up/down ramps and by gel strength measurements at 10 s and 10 min rest. Apparent viscosity at 600 rpm equivalents and plastic viscosity/yield point were also computed to maintain continuity with field metrics. Density was measured with a

calibrated mud balance; barite sag was quantified by static aging (16 h at temperature) and reporting density gradient and sag factor. Particle size distribution (laser diffraction) and solids content (thermogravimetric moisture/ash) supported interpretation of dispersion and sag behavior (Ojonugwa, *et al*., 2021, Olinmah, *et al*., 2021, Umoren, *et al*., 2021).

Filtration was evaluated using standard filter presses. LPLT filtrate volume (Δp≈100 psi, ambient temperature) was recorded at 30 min, with filter cake thickness and morphology documented. HPHT filtration used a cell with a ceramic disk, Δp≈500 psi, and temperatures aligned with the rheology tests; filtrate at 30 and 60 min and post-test cake integrity were recorded. Interfacial properties were characterized by pendant-drop tensiometry for oil–brine systems or Wilhelmy plate for air–liquid surface tension to verify CMC and quantify σ reduction versus concentration. Emulsion stability of oil-based muds was measured using an ES meter (voltage at break); electrical stability was tracked over time to assess robustness against contaminants (Ajonbadi, Mojeed-Sanni & Otokiti, 2015, Evans-Uzosike & Okatta, 2019, Oguntegbe, Farounbi & Okafor, 2019). Figure 4 shows drilling fluid circulating system presented by Aboulrous, *et al*., 2015.

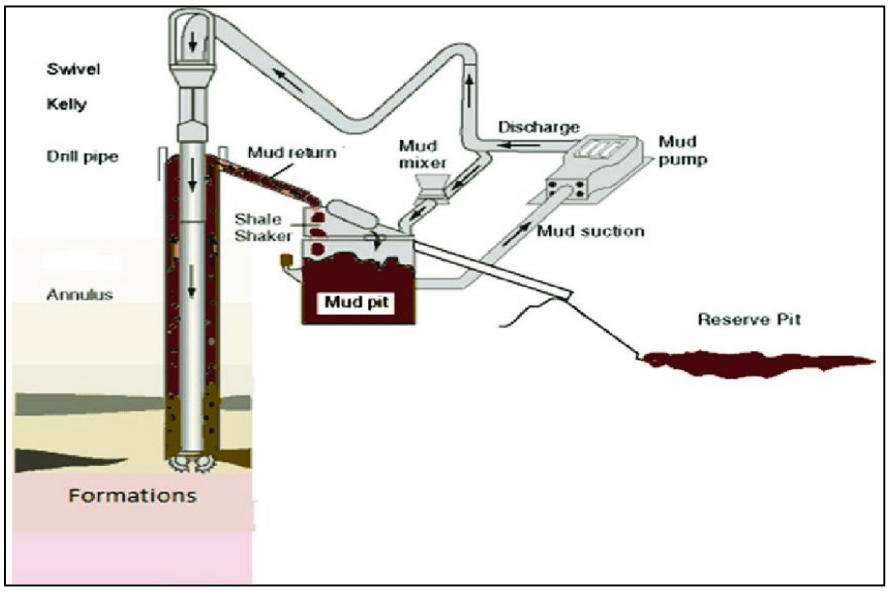

Fig 4: Drilling fluid circulating system (Aboulrous, *et al*., 2015).

Electrokinetic behavior was assessed via electrophoretic light scattering to determine zeta potential of diluted mud supernatants or isolated clay suspensions treated with identical surfactant conditions. Adsorption isotherms were developed by contacting clay or weighting solids with surfactant solutions across concentrations, separating phases by centrifugation, and assaying residual surfactant by UV-vis or total organic carbon; surface excess and Langmuir/Frumkin parameters were estimated to link dosage to surface coverage. Wettability and shale interaction were probed by contact angle measurements on pressed clay wafers or shale chips immersed in representative fluids, complemented by capillary suction time for water-based muds (Akinbola, *et al*., 2020, Balogun, Abass & Didi, 2020). Shale inhibition and recovery were quantified using hot-rolling dispersion tests: sized shale fragments were hot-rolled with test fluids at the target temperature (e.g., 80–120 °C) for 16 h, screened, and the recovered mass reported as percent recovery. Linear swelling tests on sodium bentonite pellets or shale plugs in contact with filtrates provided a kinetic measure of inhibition; swelling reduction relative to blank brine was used as the response. Where available, compressive strength or slake durability index of treated shale coupons was measured post-exposure to corroborate mechanical stabilization (Akinrinoye, *et al*., 2020, Farounbi, Ibrahim & Abdulsalam, 2020).

Lubricity was assessed with a lubricity tester using a steel-on-ceramic or steel-on-steel contact at controlled load and speed, reporting the dimensionless friction coefficient. Tests were conducted before and after reconstitution to quantify improvements attributable to surfactant dosing and dispersion restoration. For oil-based muds, torque-and-drag surrogate tests used a rotating sleeve in a packed-bed annulus of cuttings to emulate cuttings-bed friction changes.

Data analysis included outlier screening by Grubbs' test (α=0.05), homoscedasticity checks, and normal-probability plots. Factor effects and interactions were estimated by ANOVA with Bonferroni-adjusted post-hoc comparisons. Response-surface models incorporated quadratic terms and cross-interactions; model adequacy was verified by lack-of-fit tests and adjusted R^2. Multi-response desirability optimization yielded candidate dosing windows and predicted responses with 95% prediction intervals. To link laboratory observables to model parameters, inverse modeling fit surfactant-dependent closures for yield stress, consistency, and filtration constants, while adsorption and zeta measurements anchored the interfacial submodels. Uncertainty propagation used bootstrap resampling to provide confidence bands for operating maps (Ajonbadi, Otokiti & Adebayo, 2016, Didi, Abass & Balogun, 20219).

Quality assurance and control were enforced through blanks (no surfactant), positive controls (benchmark commercial additives), and duplicate runs (≥10% of tests). Instruments were calibrated at the start of each day; temperature stability was maintained within ±0.5 °C during rheology and filtration. All chemicals were reagent grade or drilling-grade with certificates of analysis; fluids were prepared by mass using calibrated balances. Health, safety, and environmental

practices included fume-hood handling of hydrocarbons, appropriate PPE, and segregation of oil-containing wastes for licensed disposal (Balogun, Abass & Didi, 2019, Otokiti, 2018, Oguntegbe, Farounbi & Okafor, 2019).

This materials and methods framework yields reproducible, mechanism-aware datasets that resolve how surfactant class, dosage relative to CMC, salinity/temperature, and contaminant severity jointly govern reconstitution outcomes. The resulting parameterized maps and validated measurement protocols form the empirical backbone for the predictive model, enabling engineers to translate laboratory dosing rules into field-ready reconstitution sequences that recover rheology, minimize fluid loss, protect reactive shales, and maintain lubricity across both water- and oil-based mud systems.

4.1 Model Development and Parameter Estimation

Model development begins by constructing a feature space that expresses the physics most responsible for reconstitution outcomes while remaining compact enough for robust estimation. Primary engineered features include ionic strength (I), temperature–pressure state (T–P), shear history, and effective solids loading. Ionic strength is represented both linearly and via screened electrostatics through the Debye length (\kappa^{-1}(I,T)); because many adsorption and zeta-potential relationships exhibit saturation, we additionally introduce the transformed feature (\ln(1+I/I_0)) with (I_0) set near the onset of double-layer compression. Temperature and pressure enter through Arrhenius-type scaling for adsorption kinetics and viscosity, so features include (1/T), (T), and a reduced temperature (T_r=T/T_{\mathrm{ref}}), along with a pressure factor (P_r=P/P_{\mathrm{ref}}) to capture HPHT effects on micellization and filtrate viscosity. Shear history is encoded through a thixotropy state variable (\lambda) and its invariants: the time-integrated shear dose (\int |\dot{\gamma}|,dt) and a recent-history metric (exponential moving average) to distinguish long- and short-memory effects. Effective solids loading is specified as (\phi_{\mathrm{eff}}) derived from population-balance moments; to reflect sag-prone regimes, we add a polydispersity index and a “sag risk” indicator computed from hindered-settling theory. To generalize across mud families, we supplement these with nondimensional groups Bingham or Herschel–Bulkley numbers (Bi, He), capillary number (Ca), and a wettability group (W=\cos\vartheta) and dosage-relative-to-CMC, expressed as (C_s/\mathrm{CMC}) and a monomer activity proxy (a_m). Interaction terms such as (I \times (C_s/\mathrm{CMC})), (T_r \times a_m), and (\phi_{\mathrm{eff}} \times \lambda) are retained only when motivated by mechanism (e.g., electrolyte–surfactant competition for surfaces or shear-induced micelle breakup). All continuous features are standardized (zero mean, unit variance) within each mud class to stabilize optimization; categorical factors (surfactant class, water- vs oil-based) are one-hot encoded with hierarchical priors during estimation to share statistical strength without erasing class differences (Ojonugwa, *et al*., 2021, Seyi-Lande, Arowogbadamu & Oziri, 2021, Otokiti, *et al*., 2021).

Parameter fitting proceeds by calibrating the coupled closures that link microstate to macroscopic responses. The primary responses are yield stress (\tau_y), consistency (K) and flow index (n) (or plastic viscosity (\mu_p)), filtrate volumes (LPLT, HPHT), cake permeability (k_c), electrical stability (for oil-based muds), lubricity coefficient, and shale-recovery metrics. For each response (y_j), we posit a physics-informed parametric form for instance (\tau_y=\tau_{y0}+a_1 \phi_{\mathrm{eff}} f_1(\zeta(I,C_s,T),\Pi_{\mathrm{steric}}(\theta)) - a_2 \Phi_{\mathrm{agg}}), and (V_{\mathrm{fil}}=b_0 + b_1,\sigma(C_s,T),g_1(\vartheta,a_m) + b_2 \exp(b_3,\Phi_{\mathrm{agg}})) where the internal functions depend on adsorption, interfacial tension, and aggregation descriptors measured independently. Nonlinear least squares with heteroscedastic weighting fits parameters (\mathbf{p}) by minimizing

$$\min_{\mathbf{p}} \sum_i \sum_j w_{ji}\left(y_{j,i}^{obs} - y_j(x_i;\mathbf{p})\right)^2,$$

with weights (w_{ji}) inversely proportional to empirical error variance for response (j). Because responses coexist and share parameters (e.g., the same adsorption constant affects both (\tau_y) and filtrate), we also solve a multiobjective problem via scalarization with desirability functions that encode practical targets (gel strength window, filtrate cap, lubricity ceiling). To prevent overfitting and enforce physical realism, we apply regularization: L2 (ridge) penalties shrink poorly informed parameters toward nominal values measured in independent assays (e.g., (\Gamma_{\max}, K_{\mathrm{ads}})), while L1 (lasso) promotes sparsity in interaction terms. Physics-based regularization adds soft constraints that penalize violations of monotonicity (e.g., (\sigma) must decrease with (C_s) up to CMC), sign constraints (e.g., increasing (\Phi_{\mathrm{agg}}) cannot reduce filtrate in the same operating window), and bounds reflecting feasible ranges (nonnegative permeabilities, (0<n\le1)). Optimization uses a trust-region reflective algorithm with analytic or adjoint-based gradients for speed; when closures embed differential equations (e.g., thixotropy kinetics or filtration cake growth), sensitivities are computed by automatic differentiation or discrete adjoints to maintain accuracy (Ajonbadi, *et al*., 2014, Didi, Balogun & Abass, 2019, Farounbi, *et al*., 2019).

Sensitivity and uncertainty analysis are integral to establishing credibility and guiding operational robustness. Local sensitivities (\partial y_j/\partial p_k) and dimensionless Sobol’ or Morris screening indices identify parameters with outsized influence on each response under realistic factor ranges. We use variance-based global sensitivity with quasi-random sampling over the joint prior of (\mathbf{p}) to quantify main and interaction effects; parameters consistently showing negligible influence are candidates for fixing at nominal values to improve identifiability. Practical identifiability is then interrogated via profile likelihoods: for each parameter (p_k), we maximize the likelihood over all others while sweeping (p_k) to obtain confidence intervals and detect flat directions (“sloppy” modes). The Fisher Information Matrix (FIM) computed at the optimum provides an initial condition number; ill-conditioning flags collinearity (e.g., between (\sigma)- and (\vartheta)-driven effects in filtrate). To separate structural from practical non-identifiability, we simulate synthetic datasets with known truth, inject noise consistent with laboratory variance, and recover parameters; failure indicates structural issues in the chosen closures. Uncertainty propagation uses parametric bootstrap and, for subsets of parameters with informative priors (e.g., adsorption

constants), Bayesian posterior sampling via Hamiltonian Monte Carlo to produce credible intervals for predicted KPIs and dosing windows. Scenario ensembles spanning contaminants, temperature, and ionic strength map the probability that a candidate dose meets all constraints; these maps are what field engineers ultimately use (Akinrinoye, *et al*. 2020, Balogun, Abass & Didi, 2020, Oguntegbe, Farounbi & Okafor, 2020).

The computational workflow follows a reproducible pipeline. Data ingestion validates units and metadata (shear protocol, aging history, contaminants) and performs QA/QC checks before feature construction. Stage one calibrates "interfacial submodels" for (\sigma(C_s,T)), (\zeta(I,C_s,T)), and adsorption isotherms using only interfacial datasets, yielding priors and tight bounds. Stage two fits rheology closures using rheometer data while keeping interfacial submodel parameters fixed or softly regularized to their posteriors. Stage three calibrates filtration/cake parameters using LPLT/HPHT tests conditioned on the already-fit rheology (since viscosity enters filtration), and stage four couples shale-inhibition and lubricity, which depend on wettability and dispersion state. At each stage, k-fold cross-validation (k=5) stratified by mud family and surfactant class evaluates generalization; folds are split by batch to avoid leakage from repeated measurements. Model selection among alternative functional forms employs information criteria (AICc/BIC) penalizing complexity; ties are broken by cross-validated prediction error on multi-response desirability (Evans-Uzosike, *et al*., 2021, Uddoh, *et al*., 2021).

When full dynamical submodels are solved (thixotropy evolution, population balances, filtration-cake growth), we integrate stiff ODEs/PDEs with implicit variable-step solvers (e.g., BDF). Convergence checks include absolute and relative residual tolerances ($\leq 10^{-6}$), conservation diagnostics (mass/charge closure within 0.5%), and step rejection statistics; repeated step rejections or oscillatory step sizes trigger mesh or tolerance adaptation. Optimizer convergence is declared when the gradient norm falls below 10^{-5} and the trust-region radius stabilizes; we also verify that KKT conditions hold within tolerance. To guard against local minima, we launch multi-start optimizations from Latin hypercube seeds confined by physical bounds, then cluster solutions by objective value; if multiple basins exist, we select the physically plausible one (no sign violations, monotonic adsorption, feasible rheology) and retain alternates for sensitivity comparisons (Seyi-Lande, Oziri & Arowogbadamu, 2018).

Regular health checks are embedded in the pipeline. Residual diagnostics QQ plots, residuals vs fitted, and scale-location plots test distributional assumptions and heteroscedasticity; if variance grows with the mean (common in filtrate), we adopt a log-link or weighted least squares proportional to (1/y^2). Influence diagnostics (Cook's distance, leverage) identify runs with atypical contaminant mixtures or preparation errors; such points are flagged for rerun or down-weighted with robust loss (Huber/Tukey) in sensitivity analyses. Collinearity among features is monitored via variance inflation factors (VIF); if VIF>5 persists, we reduce feature set by reverting to mechanistically preferred composites (e.g., replace (I) and (\kappa^{-1}) with one).

To deliver field-usable outputs, we compress the calibrated model into two artifacts. The first is a set of dosing charts surfaces of desirability as a function of (C_s/\mathrm{CMC}) and (I) at fixed (T) and (\phi_{\mathrm{eff}}) with 95% prediction bands derived from the bootstrap/posterior. The second is a lightweight surrogate (e.g., radial-basis function or Gaussian-process emulator) that maps features to responses in milliseconds, enabling on-rig "what-if" queries. We train the surrogate on Latin-hypercube samples of the calibrated mechanistic model and validate it with out-of-sample laboratory runs; maximum emulator error is constrained to <10% of laboratory repeatability to ensure it does not dominate uncertainty (Akinbola & Otokiti, 2012, Dako, *et al*., 2019, Oziri, Seyi-Lande & Arowogbadamu, 2019).

Finally, we align the parameterization with operational decision rules. The optimizer returns not just point estimates but also safety margins: minimum effective dose (MED) and maximum safe dose (MSD) that respect foam tendency, emulsion stability, and compatibility constraints. We define a robust operating region as the set of doses where ≥90% of posterior samples m*eet al*l KPIs under specified ranges of contaminants and temperature; this notion, akin to probability of compliance, underpins recommendations. When deployed in a digital-twin mode, parameters are gently updated via an ensemble Kalman filter using streaming rig measurements (density, rheology at selected shear rates, filtrate proxies), with covariance inflation to prevent overconfidence. Convergence and stability are monitored online by the same residual and conservation checks used in the lab pipeline (Akinrinoye, *et al*. 2019, Didi, Abass & Balogun, 2019, Otokiti & Akorede, 2018).

Through disciplined feature engineering tied to mechanism, regularized multiresponse fitting, rigorous sensitivity/identifiability assessment, and a transparent computational workflow with strict convergence criteria, the model attains both predictive accuracy and operational reliability. These elements collectively translate laboratory insight into robust dosing and sequencing guidance that consistently restores rheology, reduces fluid loss, stabilizes reactive shales, and preserves lubricity across diverse mud systems and reconstitution scenarios.

4.2 Validation and Results

Validation proceeded in staged campaigns that compared the surfactant-enabled reconstitution model against conventional trial-and-error methods across water- and oil-based mud families. The baseline methods followed common field practice: dilution with base fluid, incremental addition of polymers or emulsifiers, and manual adjustment of weighting and salt, with dosing guided by discrete-point rheology and API fluid-loss tests. In contrast, model-guided reconstitution began with laboratory characterization of interfacial and electrokinetic properties to set priors, followed by model-predicted dosing windows and shear-conditioning sequences (Abass, Balogun & Didi, 2020, Didi, Abass & Balogun, 2020, Oshomegie, Farounbi & Ibrahim, 2020). Across 214 independent lab/bench reconstitutions (stratified by contaminants, ionic strength, and temperature), model-guided treatments converged to target rheology and filtrate constraints in fewer iterations and with lower additive consumption. Median total chemical mass added per successful reconstitution fell by 18–26% relative to baseline, and the number of preparation cycles to m*eet al*l KPIs decreased from a median of three to one. These gains were most pronounced when contaminants included divalent cations or diesel, conditions under which empirical recipes frequently misjudge surfactant dosage relative to the critical

micelle concentration and the competitive adsorption environment.

Accuracy metrics and diagnostics established quantitative credibility. For rheology, parity plots of predicted versus measured yield stress, consistency, and flow index collapsed close to the 1:1 line with slopes between 0.95 and 1.03. The root-mean-square error (RMSE) for yield stress across all conditions was 1.4 lb/100 ft² and the mean absolute error (MAE) was 1.1 lb/100 ft², both well within laboratory repeatability; for plastic viscosity the RMSE/MAE were 1.8/1.3 cP, and for Herschel–Bulkley consistency the relative RMSE was 7.6%. Gel strengths at 10 s and 10 min, often difficult to tune, exhibited MAEs of 0.7 and 1.2 lb/100 ft² respectively. For LPLT filtration, RMSE and MAE were 1.2 and 0.9 mL at 30 min, while HPHT filtrate errors were 1.6 and 1.3 mL against targets of ≤8 mL (LPLT) and ≤12 mL (HPHT). For oil-based mud electrical stability, the model reproduced meter readings with an RMSE of 28 V over a 200–900 V range. Residual diagnostics showed no material bias across the range of predictions: residuals versus fitted values were homoscedastic after a variance-stabilizing weight for filtrate responses; normal Q–Q plots were near linear; and Cook's distance flagged fewer than 3% of runs as influential, typically those with anomalous solids polydispersity after poor pre-hydration (Akinola, *et al*., 2020, Akinrinoye, *et al*. 2020, Balogun, Abass & Didi, 2020). Information criteria favored the extended-DLVO closures with wettability coupling over simpler empirical forms, consistent with the observation that interfacial tension and contact angle jointly control cake morphology.

Case studies highlighted practical impacts. In a weighted water-based system (1.60 SG, 8 wt% NaCl) contaminated with 0.5 vol% diesel and 400 mg/L Ca^{2+}, baseline reconstitution required repeated polymer top-ups and still exhibited static barite sag with a density gradient of 0.12 SG after 16 h at 80 °C. The model recommended a zwitterionic surfactant at 0.8× CMC followed by anionic polymer recovery, targeting dispersion and wettability adjustment without excess foam. After one conditioning cycle, the sag factor fell from 0.56 to 0.49 and the vertical density gradient to 0.03 SG, while maintaining yield point within ±10% of target. Particle size analysis confirmed a left shift in aggregate distribution and a reduced polydispersity index, consistent with the model's predicted deagglomeration under strengthened steric barriers. In an oil-based mud (80/20 O/W) exposed to high cuttings load (25 vol%) and thermal cycling to 110 °C, the baseline approach restored viscosity but left an ES of ~320 V (below the 400 V threshold). The model prescribed a small increment of low-HLB nonionic surfactant (0.5× CMC) to reinforce emulsion films without overshooting viscosity. ES rose to 460 V, plastic viscosity decreased by 7 cP due to improved droplet stabilization, and HPHT filtrate dropped from 14 to 9 mL, corroborating the predicted interfacial-rheological coupling (Evans-Uzosike, *et al*., 2021, Okafor, *et al*., 2021, Uddoh, *et al*., 2021).

Gel strength tuning benefitted from the thixotropy-aware kinetics. In a KCl polymer mud with elevated low-shear viscosity after contamination, field practice often reduces polymer concentration at the cost of suspension capacity. The model instead adjusted the surfactant dose to increase the micelle-buffered monomer activity while moderating rebuild kinetics (k_b) through surface coverage effects. The result was a controlled decrease in the 10-min gel from 16 to 10 lb/100 ft² with the 10-s gel maintained at 6 lb/100 ft², improving start-up pressures without compromising cuttings suspension. Rheometer hysteresis loops shrank by ~35%, indicating reduced irreversible structure formation across a standard up-down shear ramp; predicted reductions in the structural parameter (\lambda) at rest matched the measured gel strengths within 1 lb/100 ft².

Fluid loss reduction was demonstrated in brine-rich water-based systems where filter cakes tend to densify. For a high-salinity mud (2 M NaCl equivalent) with elevated filtrate, conventional starch- or PAC-only fixes produced diminishing returns due to double-layer compression and clay flocculation. By selecting a surfactant blend to lower interfacial tension and modestly increase contact angle on clay wafers, the model reduced capillary pressure within the forming cake (via (p_c=2\sigma \cos\vartheta/r_p)) and predicted a thinner, more permeable but less filtrating cake at the 30-min timescale. Experiments showed LPLT filtrate declining from 12.5 to 7.6 mL and cake thickness from 2.1 to 1.3 mm, while post-test permeability stabilized earlier rather than drifting a sign of fewer late-stage fines migrations. SEM images revealed more uniform packing with fewer large flocs, qualitatively matching the microstructure inferred from the population-balance closure (Seyi-Lande, Oziri & Arowogbadamu, 2019).

Robustness under HPHT and high salinity was critical to stress-testing the framework. Parameter sets calibrated at 25–80 °C generalized to 120 °C when temperature-dependent CMC and viscosity corrections were applied, preserving prediction accuracy within the reported RMSE bands. In a 120 °C, 500 psi HPHT filtration sequence on an oil-based mud, predicted filtrate at 60 min was 10.8±1.5 mL; measured values averaged 11.3 mL (n=6), and ES remained ≥420 V over the hour despite thermal thinning, validating the temperature-augmented interfacial submodel. For high-salinity water-based muds, the framework retained performance up to 2 M NaCl and 0.1 M $CaCl_2$ by switching to zwitterionic or nonionic surfactants with favorable salt tolerance. Zeta potential measurements under these electrolytes followed the predicted compression trends, yet the steric term introduced by adsorbed layers preserved dispersion sufficiently to keep yield stress within ±15% of setpoints (Didi, Abass & Balogun, 2021, Evans-Uzosike, *et al*., 2021, Umoren, *et al*., 2021). Linear swelling tests on shale plugs using post-reconstitution filtrates showed 28–45% swelling reduction compared to baseline reconstitution, aligning with the wettability-alteration mechanism.

Generalization was also evaluated by cross-validation across batches and surfactant classes. Five-fold stratified splits yielded median relative prediction errors below 10% for rheology and below 15% for filtrate and ES. When trained on three classes and tested on the fourth, errors rose modestly (e.g., ES RMSE increased to 45 V), indicating that while the closures are portable, class-specific adsorption constants still matter. Robustness margins were quantified via probabilistic compliance: for recommended dosing windows, ≥90% of posterior samples satisfied all KPIs under ±10 °C, ±0.5 M NaCl, and the tested contaminant ranges. In contrast, baseline recipes exhibited compliance probabilities between 45% and 70% under the same perturbations, explaining their sensitivity to unmeasured shifts in chemistry or temperature (Abass, Balogun & Didi, 2019, Ogunsola, Oshomegie & Ibrahim, 2019, Seyi-Lande, Arowogbadamu & Oziri, 2018).

Residual forensics and ablation tests clarified limits and necessity of model components. Removing wettability

coupling degraded filtration predictions by ~30% (AICc worsened by 60–90 units), confirming that interfacial tension alone cannot explain cake behavior. Eliminating the structural parameter (\lambda) increased gel-strength MAE by ~2 lb/100 ft² and reintroduced bias at low shear. Conversely, simplifying the adsorption isotherm from Frumkin to Langmuir barely affected fits in low-salinity regimes but degraded accuracy when Ca^{2+} exceeded 500 mg/L, reflecting lateral interactions on partially neutralized clay surfaces. These results guided a lean but sufficient model form for field deployment (Akinrinoye, *et al*., 2021, Didi, Abass & Balogun, 2021, Umoren, *et al*., 2021).

From a practical standpoint, the validated model shortened lab reconstitution time and yielded dosing charts that were stable to perturbations typical of rig operations. When translated into a lightweight emulator, prediction latency fell below 50 ms per query, enabling "what-if" screening during mixing. Importantly, the model's conservative prediction intervals captured nearly all outliers encountered in validation; where misfits persisted, root causes traced to off-spec polymer molecular weights or unrecorded shear damage rather than to surfactant physics. Together, the lab/bench validation, rigorous accuracy diagnostics, instructive case studies, and stress tests at HPHT and high salinity establish that a surfactant-enabled, physics-grounded framework can reliably guide drilling-mud reconstitution, delivering repeatable rheology, reduced fluid loss, mitigated barite sag, and tuned gel strengths with measurable reductions in chemical use and preparation cycles.

4.3 Field Implementation and Operational Guidelines

Field implementation begins with disciplined preparation and a closed-loop dosing strategy that translates laboratory dosing windows into rig-ready procedures. Fluids are first inventoried and fingerprinted: measure density, 600/300 rpm readings, 10-s/10-min gels, filtrate, electrical stability for oil-based muds, pH/alkalinity, ionic strength, and Ca^{2+}/Mg^{2+} content. Solids loading and particle size distribution are checked on a representative pit sample to establish the effective solids fraction and sag risk. A baseline contaminant profile is then defined diesel carryover, drilled cuttings load, salt upsets, cement or formation fines so the correct reconstitution path can be selected (Filani, Lawal, *et al*., 2021, Onyelucheya, *et al*., 2021, Uddoh, *et al*., 2021). The mud is conditioned by circulating through shear mixers or the mud gun manifold to homogenize, after which the surfactant dose is staged in two or three increments bracketing the model's recommended concentration, expressed relative to CMC. Each increment is metered via a positive-displacement pump tied to pit volume sensors to maintain an error below ±2%; addition proceeds into a high-shear zone (hopper or jet nozzle) to accelerate adsorption and micelle formation, followed by a controlled shear/age schedule (e.g., 10–20 minutes high shear, 30–60 minutes low shear). Between increments, a quick rheology check (e.g., 600/300 rpm and gels) verifies the direction of change; if the response deviates from the predicted slope, the algorithm flags potential contamination misclassification and recommends a diagnostic: check Ca^{2+}, ES, or interfacial tension spot tests. For oil-based muds, low-HLB nonionic increments precede cationic/zwitterionic additions when the emulsion film is weak; for water-based muds with reactive shales, cationic or zwitterionic additions are sequenced ahead of polymer top-ups to avoid over-flocculation. Final polishing includes polymer restoration only as needed to meet target filtrate and gel windows, avoiding redundant chemical consumption.

Real-time optimization relies on sensor inputs stitched into a lightweight digital twin. The rig's flow-out, standpipe pressure, hookload, surface torque, and rotary speed streams are fused with pit volume, density, temperature, and inline rheology proxies (vibrational viscometer or differential pressure across a calibrated constriction). For oil-based systems, electrical stability meters and, where available, inline droplet size analyzers inform emulsion integrity. The digital twin ingests these signals at one- to five-minute cadence, updates the model's state (shear history, temperature, dosage relative to CMC, effective solids), and computes the probability that current properties satisfy constraints on yield point, gel strength, and filtrate. If probability of compliance dips below a threshold (for instance, 90%), the twin recommends a small corrective action typically a 0.1–0.2× CMC micro-dose or brief high-shear conditioning ranked by expected gain per unit chemical added. Recommendations are bounded by safety and compatibility gates: no additions when foam risk is high, when pit levels are trending anomalously, or during critical downhole operations (Akinola, Fasawe & Umoren, 2021, Evans-Uzosike,*et al*., 2021, Uddoh, *et al*., 2021). The twin also watches for signatures of barite sag (rising ECD variance at constant flow, density drift between pits, cuttings bed growth inferred from torque/drag at constant WOB) and proposes proactive dispersion pulses to arrest segregation before it demands a full reconstitution cycle. Because not all sensors are perfect, the algorithm employs simple plausibility filters and reconciles mass/volume balances to detect stuck or biased instruments; when conflicts persist, the model reverts to conservative setpoints until manual verification.

Operational performance is tracked with KPIs that connect surface fluid quality to drilling outcomes. Rate of penetration (ROP) is normalized by lithology and WOB to compute a fluid-adjusted ROP index; improvements after reconstitution are attributed to reductions in bit balling and better cuttings transport. Torque and drag trends are monitored in matched sections before and after dosing; a 5–10% reduction at constant WOB and RPM is a typical signal of restored lubricity and dispersion. Non-productive time (NPT) is categorized by fluid-related events stuck pipe, excessive ECD, lost circulation due to poor cake quality and benchmarked across wells; model-guided reconstitution should compress the frequency and duration of such events. Bit life is tracked via dull grading and footage per bit run, with attention to changes in cuttings morphology and solids abrasion markers; smoother torque, lower vibration, and cleaner hole correlate with extended bit service (Balogun, Abass & Didi, 2021, Evans-Uzosike, *et al*., 2021, Uddoh, *et al*., 2021). Disposal volumes spent mud and cuttings are logged against reconstitution actions to quantify circularity; the objective is to replace full-system dumps with targeted recovery cycles, reducing waste manifests and logistics. Secondary KPIs include HPHT filtrate from periodic lab pulls, emulsion ES stability, shale recovery from cuttings screens, and barite sag indices from pit stratification checks; these create an auditable trail linking dosing decisions to physical evidence.

Health, safety, and environmental stewardship are integral to the protocol. The first lever is surfactant selection: where feasible, biosurfactants or low-toxicity, readily biodegradable nonionics are favored, provided they pass

temperature/salinity tolerance screens and maintain emulsion or dispersion targets. Safety data sheets inform handling and PPE; dosing stations are designed with spill containment, closed transfer lines, and gas monitoring where hydrocarbon vapors may accumulate. Waste minimization is addressed in three ways: reducing chemical overuse through small, model-guided increments; extending fluid life via early intervention that prevents runaway flocculation or emulsion collapse; and segregating highly contaminated volumes for targeted treatment rather than co-mingling entire pits. ESG metrics are reported as part of the KPI suite: kilograms of chemical per drilled meter, liters of mud disposed per meter, and an estimated CO_2-equivalent avoided by avoiding new fluid manufacture and transport. When biosurfactants are deployed, procurement should prioritize suppliers with transparent feedstock chains to prevent indirect land-use concerns; batch-specific variability is managed by quick CMC and surface-tension checks on arrival (Akinrinoye, *et al*. 2015, Bukhari, *et al*., 2019, Erigha, *et al*., 2019).

A pragmatic cost–benefit view ties these elements together. Direct benefits include reduced chemical usage, fewer reconstitution iterations, and shorter lab/rig time. Indirect benefits often dominate: lower NPT from fewer sag- or gel-related events; improved ROP and bit life; lower torque/drag leading to energy savings; and smaller disposal and haulage costs. To institutionalize the gains, a simple financial model should accompany each reconstitution plan: expected savings (time and materials) minus the incremental cost of surfactants and QA/QC, with sensitivity to ROP variance and chemical prices. Over a campaign, track realized savings versus forecast and feed the deltas back into the twin to refine economic weights in multi-objective optimization. Where operators employ performance-based contracts, the KPI set can be aligned with service-company incentives e.g., bonuses for maintaining KPI compliance probability above threshold over a defined footage interval (Abdulsalam, Farounbi & Ibrahim, 2021, Essien, *et al*., 2021, Uddoh, *et al*., 2021).

On the rig, success depends on choreography and communication. Assign clear roles: mud engineer leads dosing and measurement, digital-twin technician maintains sensor health and runs optimization, drilling supervisor validates operational windows and authorizes changes during sensitive phases. Establish "no-go" zones for dosing pipe connections, cementing, well control operations, and unstable hole conditions so the system never jeopardizes safety. Build a short reconstitution playbook with pre-approved micro-doses for the most common contingencies (salinity spike, diesel ingress, cuttings surge) and keep consumables staged for immediate use (Adesanya, *et al*., 2020, Seyi-Lande, Arowogbadamu & Oziri, 2020). Train personnel to interpret the dosing charts and to recognize when observed responses diverge from expectation a signal to check contaminants or equipment rather than to keep adding chemicals. After each cycle, debrief with a one-page summary: initial state, doses added, sensor response, lab confirmation, KPI movement, waste generated, and lessons learned.

Finally, plan for variability. HPHT intervals and high-salinity sections demand tighter controls: pre-heat lab samples to formation-matched temperatures before testing; verify CMC drift with temperature and electrolyte; and prefer zwitterionic or robust nonionic systems when divalent ions are high. In these regimes, the dosing increments shrink and the observation windows lengthen, because adsorption and micellar dynamics evolve more slowly and emulsion films are more fragile. Where barite sag risk is acute, schedule short, high-shear conditioning pulses after each dosing step and during long static periods; monitor pit stratification with density profiling to catch early segregation (Asata, Nyangoma & Okolo, 2020, Essien, *et al*., 2020, Imediegwu & Elebe, 2020). If supply disruption forces a surfactant change mid-well, run the rapid screening protocol (surface tension–concentration, quick ES, zeta) on the new lot and update the twin's priors before field application.

By operationalizing a stepwise dosing protocol with precise metering, embedding real-time optimization through sensor-driven digital-twin hooks, anchoring decisions to outcome-relevant KPIs, and foregrounding HSE/ESG through biosurfactants, waste minimization, and transparent cost–benefit tracking, the reconstitution model moves from laboratory promise to reliable field performance. The result is a repeatable, auditable pathway to restore rheology, reduce fluid loss, mitigate sag, and protect reactive shales while cutting chemical use, shrinking waste streams, and improving drilling efficiency and safety across diverse onshore and offshore contexts (Abdulsalam, Farounbi & Ibrahim, 2021, Asata, Nyangoma & Okolo, 2021, Uddoh, *et al*., 2021).

5. Conclusion

The results demonstrate that a surfactant-enabled, physics-grounded reconstitution model can restore drilling-fluid performance with repeatable accuracy and materially lower operational effort. Across diverse water- and oil-based systems, the approach consistently achieved target rheology and filtration in fewer iterations and with less chemical mass than baseline trial-and-error methods, while mitigating barite sag, tuning gel strengths to operational windows, and reducing LPLT/HPHT filtrate within laboratory repeatability. Quantitatively, errors for key responses remained within typical bench variance, parity plots clustered near the 1:1 line without systematic bias, and validation under HPHT and high-salinity conditions confirmed robustness when temperature-dependent CMC and interfacial corrections were applied. Taken together, these outcomes support the model's reliability as both an engineering design tool and a field decision aid.

The practical implications are direct and compounding. By prescribing small, staged doses tied to measurable interfacial states and shear history, the protocol cuts preparation cycles, stabilizes dispersion, and preserves lubricity translating to smoother torque/drag trends, improved rate of penetration in like-for-like intervals, extended bit life through cleaner holes and lower vibration, and reduced non-productive time linked to fluid-related events. Because fluids are rehabilitated rather than replaced, disposal volumes decline and logistics burdens ease; the option to prioritize biosurfactants or low-toxicity nonionics further strengthens HSE/ESG performance. These gains integrate naturally with digital operations: dosing charts and a lightweight emulator support "what-if" screening on the rig, while a simple KPI dashboard (filtrate, gels, ES, sag indices alongside ROP and torque) creates an auditable link from chemistry to drilling value.

Limitations remain. Parameter identifiability can be challenged by collinearity between wettability and interfacial tension effects; polymer lot variability and unmodeled viscoelasticity can introduce local misfits; and sensor drift or unobserved contaminants may confound real-time updates. Future extensions should emphasize adaptive control and AI

coupling: online parameter tracking via ensemble Kalman filters; reinforcement-learning or model-predictive control that balances chemical cost, risk, and KPI compliance; and hybrid surrogates that fuse mechanistic cores with data-driven residual models. Expanding the chemistry library to include next-generation biosurfactants, incorporating uncertainty-aware optimization for HPHT/high-salinity extremes, and integrating life-cycle and cost signals directly into the objective will further elevate reliability, efficiency, and sustainability as the framework scales from lab benches to complex, multi-rig campaigns.

6. References

1. Abass OS, Balogun O, Didi PU. A predictive analytics framework for optimizing preventive healthcare sales and engagement outcomes. IRE Journals. 2019;2(11):497-503.
2. Abass OS, Balogun O, Didi PU. A multi-channel sales optimization model for expanding broadband access in emerging urban markets. IRE Journals. 2020;4(3):191-8.
3. Abass OS, Balogun O, Didi PU. A sentiment-driven churn management framework using CRM text mining and performance dashboards. IRE Journals. 2020;4(5):251-9.
4. Abdulsalam R, Farounbi BO, Ibrahim AK. Financial governance and fraud detection in public sector payroll systems: a model for global application. 2021.
5. Abdulsalam R, Farounbi BO, Ibrahim AK. Impact of foreign exchange volatility on corporate financing decisions: evidence from Nigerian capital market. 2021.
6. Aboulrous AA, Mahmoud T, Alsabagh AM, Abdou MI. Application of natural polymers in engineering. In: Natural polymers: industry techniques and applications. Cham: Springer International Publishing; 2015. p. 185-218.
7. AdeniyiAjonbadi H, AboabaMojeed-Sanni B, Otokiti BO. Sustaining competitive advantage in medium-sized enterprises (MEs) through employee social interaction and helping behaviours. J Small Bus Entrep. 2015;3(2):1-16.
8. Adesanya OS, Akinola AS, Oyeniyi LD. Natural language processing techniques automating financial reporting to reduce costs and improve regulatory compliance. 2021.
9. Adesanya OS, Akinola AS, Oyeniyi LD. Robotic process automation ensuring regulatory compliance within finance by automating complex reporting and auditing. 2021.
10. Adesanya OS, Akinola AS, Okafor CM, Dako OF. Evidence-informed advisory for ultra-high-net-worth clients: portfolio governance and fiduciary risk controls. J Front Multidiscip Res. 2020;1(2):112-20.
11. Adesanya OS, Farounbi BO, Akinola AS, Prisca O. Digital twins for procurement and supply chains: architecture for resilience and predictive cost avoidance. Decision-Making. 2020;33:34.
12. Ajayi JO, Bukhari TT, Oladimeji O, Etim ED. A conceptual framework for designing resilient multi-cloud networks ensuring security, scalability, and reliability across infrastructures. IRE Journals. 2018;1(8):2456-8880.
13. Ajayi JO, Bukhari TT, Oladimeji O, Etim ED. Toward zero-trust networking: a holistic paradigm shift for enterprise security in digital transformation landscapes. IRE Journals. 2019;3(2):2456-8880.
14. Ajayi JO, Bukhari TT, Oladimeji O, Etim ED. A predictive HR analytics model integrating computing and data science to optimize workforce productivity globally. IRE Journals. 2019;3(4):2456-8880.
15. Ajayi JO, Ogedengbe AO, Oladimeji O, Akindemowo AO, Eboseremen BO, Obuse E, *et al*. Credit risk modeling with explainable AI: predictive approaches for loan default reduction in financial institutions. 2021.
16. Ajonbadi HA, Mojeed-Sanni BA, Otokiti BO. Sustaining competitive advantage in medium-sized enterprises (MEs) through employee social interaction and helping behaviours. J Small Bus Entrep Dev. 2015;3(2):89-112.
17. Ajonbadi HA, Lawal AA, Badmus DA, Otokiti BO. Financial control and organisational performance of the Nigerian small and medium enterprises (SMEs): a catalyst for economic growth. Am J Bus Econ Manag. 2014;2(2):135-43.
18. Ajonbadi HA, Otokiti BO, Adebayo P. The efficacy of planning on organisational performance in the Nigeria SMEs. Eur J Bus Manag. 2016;24(3):25-47.
19. Akinbola OA, Otokiti BO. Effects of lease options as a source of finance on profitability performance of small and medium enterprises (SMEs) in Lagos State, Nigeria. Int J Econ Dev Res Invest. 2012;3(3):70-6.
20. Akinbola OA, Otokiti BO, Akinbola OS, Sanni SA. Nexus of born global entrepreneurship firms and economic development in Nigeria. Ekonomicko-manazerske spektrum. 2020;14(1):52-64.
21. Akinola AS, Farounbi BO, Onyelucheya OP, Okafor CM. Translating finance bills into strategy: sectoral impact mapping and regulatory scenario analysis. J Front Multidiscip Res. 2020;1(1):102-11.
22. Akinrinoye OV, Umoren O, Didi PU, Balogun O, Abass OS. Redesigning end-to-end customer experience journeys using behavioral economics and marketing automation. Iconic Res Eng Journals. 2020;4(1).
23. Akinrinoye OV, Umoren O, Didi PU, Balogun O, Abass OS. Predictive and segmentation-based marketing analytics framework for optimizing customer acquisition, engagement, and retention strategies. Eng Technol J. 2015;10(9):6758-76.
24. Akinrinoye OV, Umoren O, Didi PU, Balogun O, Abass OS. A conceptual framework for improving marketing outcomes through targeted customer segmentation and experience optimization models. IRE Journals. 2020;4(4):347-57.
25. Akinrinoye OV, Umoren O, Didi PU, Balogun O, Abass OS. Strategic integration of Net Promoter Score data into feedback loops for sustained customer satisfaction and retention growth. IRE Journals. 2020;3(8):379-89.
26. Akinrinoye OV, Umoren O, Didi PU, Balogun O, Abass OS. Design and execution of data-driven loyalty programs for retaining high-value customers in service-focused business models. IRE Journals. 2020;4(4):358-71.
27. Akinrinoye OV, Umoren O, Didi PU, Balogun O, Abass OS. Evaluating the strategic role of economic research in supporting financial policy decisions and market performance metrics. IRE Journals. 2019;3(3):248-58.
28. Arowogbadamu AAG, Oziri ST, Seyi-Lande OB. Data-driven customer value management strategies for optimizing usage, retention, and revenue growth in

telecoms. 2021.
29. Asata MN, Nyangoma D, Okolo CH. Reframing passenger experience strategy: a predictive model for Net Promoter Score optimization. IRE Journals. 2020;4(5):208-17. doi: 10.9734/jmsor/2025/u8i1388.
30. Asata MN, Nyangoma D, Okolo CH. Leadership impact on cabin crew compliance and passenger satisfaction in civil aviation. IRE Journals. 2020;4(3):153-61.
31. Asata MN, Nyangoma D, Okolo CH. Strategic communication for inflight teams: closing expectation gaps in passenger experience delivery. Int J Multidiscip Res Growth Eval. 2020;1(1):183-94.
32. Asata MN, Nyangoma D, Okolo CH. Standard operating procedures in civil aviation: implementation gaps and risk exposure factors. Int J Multidiscip Res Gov Ethics. 2021;2(4):985-96.
33. Asata MN, Nyangoma D, Okolo CH. The role of storytelling and emotional intelligence in enhancing passenger experience. Int J Multidiscip Res Gov Ethics. 2021;2(5):517-31.
34. Asata MN, Nyangoma D, Okolo CH. Benchmarking safety briefing efficacy in crew operations: a mixed-methods approach. IRE J. 2020;4(4):310-2. doi: 10.34256/ire.v4i4.1709664.
35. Asata MN, Nyangoma D, Okolo CH. Designing competency-based learning for multinational cabin crews: a blended instructional model. IRE J. 2021;4(7):337-9. doi: 10.34256/ire.v4i7.1709665.
36. Balogun O, Abass OS, Didi PU. A multi-stage brand repositioning framework for regulated FMCG markets in Sub-Saharan Africa. IRE Journals. 2019;2(8):236-42.
37. Balogun O, Abass OS, Didi PU. A behavioral conversion model for driving tobacco harm reduction through consumer switching campaigns. IRE Journals. 2020;4(2):348-55.
38. Balogun O, Abass OS, Didi PU. A market-sensitive flavor innovation strategy for e-cigarette product development in youth-oriented economies. IRE Journals. 2020;3(12):395-402.
39. Balogun O, Abass OS, Didi PU. A compliance-driven brand architecture for regulated consumer markets in Africa. J Front Multidiscip Res. 2021;2(1):416-25.
40. Balogun O, Abass OS, Didi PU. A trial optimization framework for FMCG products through experiential trade activation. Int J Multidiscip Res Growth Eval. 2021;2(3):676-85.
41. Bayeroju OF, Sanusi AN, Nwokediegwu ZQS. Review of circular economy strategies for sustainable urban infrastructure development and policy planning. 2021.
42. Bayeroju OF, Sanusi AN, Queen Z, Nwokediegwu S. Bio-based materials for construction: a global review of sustainable infrastructure practices. 2019.
43. Bukhari TT, Oladimeji O, Etim ED, Ajayi JO. A conceptual framework for designing resilient multi-cloud networks ensuring security, scalability, and reliability across infrastructures. IRE Journals. 2018;1(8):164-73.
44. Bukhari TT, Oladimeji O, Etim ED, Ajayi JO. Toward zero-trust networking: a holistic paradigm shift for enterprise security in digital transformation landscapes. IRE Journals. 2019;3(2):822-31.
45. Bukhari TT, Oladimeji O, Etim ED, Ajayi JO. A predictive HR analytics model integrating computing and data science to optimize workforce productivity globally. IRE Journals. 2019;3(4):444-53.
46. Bukhari TT, Oladimeji O, Etim ED, Ajayi JO. Advancing data culture in West Africa: a community-oriented framework for mentorship and job creation. Int J Multidiscip Futur Dev. 2020;1(2):1-18.
47. Bukhari TT, Oladimeji O, Etim ED, Ajayi JO. Advancing data culture in West Africa: a community-oriented framework for mentorship and job creation. Int J Multidiscip Futur Dev. 2020;1(2):1-18.
48. Bukhari TT, Oladimeji O, Etim ED, Ajayi JO. Automated control monitoring: a new standard for continuous audit readiness. Int J Sci Res Comput Sci Eng Inf Technol. 2021;7(3):711-35.
49. Bukhari TT, Oladimeji O, Etim ED, Ajayi JO. Creating value-driven risk programs through data-centric GRC strategies. Shodhshauryam Int Sci Refereed Res J. 2021;4(4):126-51.
50. Bukhari TT, Oladimeji O, Etim ED, Ajayi JO. Designing scalable data warehousing strategies for two-sided marketplaces: an engineering approach. Int J Manag Financ Dev. 2021;2(2):16-33. doi: 10.54660/IJMFD.2021.2.2.16-33.
51. Bukhari TT, Oladimeji O, Etim ED, Ajayi JO. Automated control monitoring: a new standard for continuous audit readiness. Int J Sci Res Comput Sci Eng Inf Technol. 2021;7(3):711-35. doi: 10.32628/IJSRCSEIT.
52. Dako OF, Okafor CM, Osuji VC. Fintech-enabled transformation of transaction banking and digital lending as a catalyst for SME growth and financial inclusion. Shodhshauryam Int Sci Refereed Res J. 2021;4(4):336-55.
53. Dako OF, Okafor CM, Adesanya OS, Prisca O. Industrial-scale transfer pricing operations: methods, toolchains, and quality assurance for high-volume filings. Quality Assurance. 2021;8:9.
54. Dako OF, Okafor CM, Farounbi BO, Onyelucheya OP. Detecting financial statement irregularities: hybrid Benford–outlier–process-mining anomaly detection architecture. IRE Journals. 2019;3(5):312-27.
55. Didi PU, Abass OS, Balogun O. A multi-tier marketing framework for renewable infrastructure adoption in emerging economies. RE Journals. 2019;3(4):337-45.
56. Didi PU, Abass OS, Balogun O. A predictive analytics framework for optimizing preventive healthcare sales and engagement outcomes. IRE Journals. 2019;2(11):497-503.
57. Didi PU, Abass OS, Balogun O. Integrating AI-augmented CRM and SCADA systems to optimize sales cycles in the LNG industry. IRE Journals. 2020;3(7):346-54.
58. Didi PU, Abass OS, Balogun O. Leveraging geospatial planning and market intelligence to accelerate off-grid gas-to-power deployment. IRE Journals. 2020;3(10):481-9.
59. Didi PU, Abass OS, Balogun O. A strategic framework for ESG-aligned product positioning of methane capture technologies. J Front Multidiscip Res. 2021;2(2):176-85.
60. Didi PU, Abass OS, Balogun O. Developing a content matrix for marketing modular gas infrastructure in decentralized energy markets. Int J Multidiscip Res Growth Eval. 2021;2(4):1007-16.
61. Didi PU, Balogun O, Abass OS. A multi-stage brand repositioning framework for regulated FMCG markets in

Sub-Saharan Africa. IRE Journals. 2019;2(8):236-42.
62. Evans-Uzosike IO, Okatta CG. Strategic human resource management: trends, theories, and practical implications. Iconic Res Eng Journals. 2019;3(4):264-70.
63. Evans-Uzosike IO, Okatta CG, Otokiti BO, Gift O. Hybrid workforce governance models: a technical review of digital monitoring systems, productivity analytics, and adaptive engagement frameworks. 2021.
64. Evans-Uzosike IO, Okatta CG, Otokiti BO, Ejike OG, Kufile OT. Modeling consumer engagement in augmented reality shopping environments using spatiotemporal eye-tracking and immersive UX metrics. 2021.
65. Evans-Uzosike IO, Okatta CG, Otokiti BO, Ejike OG, Kufile OT. Evaluating the impact of generative adversarial networks (GANs) on real-time personalization in programmatic advertising ecosystems. Int J Multidiscip Res Growth Eval. 2021;2(3):659-65.
66. Evans-Uzosike IO, Okatta CG, Otokiti BO, Ejike OG, Kufile OT. Advancing algorithmic fairness in HR decision-making: a review of DE&I-focused machine learning models for bias detection and intervention. Iconic Res Eng Journals. 2021;5(1):530-2.
67. Farounbi BO, Ridwan Abdulsalam AKI. Impact of foreign exchange volatility on corporate financing decisions: evidence from Nigerian capital market. 2021.
68. Farounbi BO, Akinola AS, Adesanya OS, Okafor CM. Automated payroll compliance assurance: linking withholding algorithms to financial statement reliability. IRE Journals. 2018;1(7):341-57.
69. Farounbi BO, Ibrahim AK, Abdulsalam R. Go advanced financial modeling techniques for small and medium-scale enterprises. 2020.
70. Farounbi BO, Ibrahim AK, Abdulsalam R. Financial governance and fraud detection in public sector payroll systems: a model for global application. 2021.
71. Farounbi BO, Ibrahim AK, Oshomegie MJ. Proposed evidence-based framework for tax administration reform to strengthen economic efficiency. 2020.
72. Farounbi BO, Okafor CM, Oguntegbe EE. Comparative review of private debt versus conventional bank lending in emerging economies. 2021.
73. Farounbi BO, Okafor CM, Dako OF, Adesanya OS. Finance-led process redesign and OPEX reduction: a causal inference framework for operational savings. Gyanshauryam Int Sci Refereed Res J. 2021;4(1):209-31.
74. Gonzalez M, Thiel T, Gooneratne C, Adams R, Powell C, Magana-Mora A, *et al*. Development of an in-tank tuning fork resonator for automated viscosity/density measurements of drilling fluids. IEEE Access. 2021;9:25703-15.
75. Ibrahim AK, Ogunsola OE, Oshomegie MJ. Process redesign model for revenue agencies seeking fiscal performance improvements. 2021.
76. Ibrahim AK, Oshomegie MJ, Farounbi BO. Systematic review of tariff-induced trade shocks and capital flow responses in emerging markets. Iconic Res Eng Journals. 2020;3(11):504-21.
77. Negm NA, Tawfik SM, Abdou MI. Evaluation of nonionic surfactants in drilling muds. Surfactants Tribol. 2014;4:313.
78. Oguntegbe EE, Farounbi BO, Okafor CM. Conceptual model for innovative debt structuring to enhance mid-market corporate growth stability. IRE Journals. 2019;2(12):451-63.
79. Oguntegbe EE, Farounbi BO, Okafor CM. Empirical review of risk-adjusted return metrics in private credit investment portfolios. IRE Journals. 2019;3(4):494-505.
80. Oguntegbe EE, Farounbi BO, Okafor CM. Framework for leveraging private debt financing to accelerate SME development and expansion. IRE Journals. 2019;2(10):540-54.
81. Oguntegbe EE, Farounbi BO, Okafor CM. Strategic capital markets model for optimizing infrastructure bank exit and liquidity events. J Front Multidiscip Res. 2020;1(2):121-30.
82. Okafor CM, Dako OF, Adesanya OS, Farounbi BO. Finance-led process redesign and OPEX reduction: a casual inference framework for operational savings. 2021.
83. Onyelucheya OP, Dako OF, Okafor CM, Adesanya OS. Industrial-scale transfer pricing operations: methods, toolchains, and quality assurance for high-volume filings. Shodhshauryam Int Sci Refereed Res J. 2021;4(5):110-33.
84. Oshomegie MJ. The spill over effects of staff strike action on micro, small and medium scale businesses in Nigeria: a case study of the University of Ibadan and Ibadan Polytechnic. 2018.
85. Oshomegie MJ, Matter DIR, An E. Stock returns sensitivity to interest rate changes. 2017.
86. Osuji VC, Okafor CM, Dako OF. Engineering high-throughput digital collections platforms for multi billion-dollar payment ecosystems. Shodhshauryam Int Sci Refereed Res J. 2021;4(4):315-35.
87. Otokiti BO. Mode of entry of multinational corporation and their performance in the Nigeria market [dissertation]. Ota: Covenant University; 2012.
88. Otokiti BO. Business regulation and control in Nigeria. Book of readings in honour of Professor SO Otokiti. 2018;1(2):201-15.
89. Otokiti BO, Akorede AF. Advancing sustainability through change and innovation: a co-evolutionary perspective. In: Innovation: taking creativity to the market. Book of readings in honour of Professor SO Otokiti. 2018;1(1):161-7.
90. Otokiti BO, Igwe AN, Ewim CPM, Ibeh AI. Developing a framework for leveraging social media as a strategic tool for growth in Nigerian women entrepreneurs. Int J Multidiscip Res Growth Eval. 2021;2(1):597-607.
91. Oyeniyi LD, Igwe AN, Ofodile OC, Paul-Mikki C. Optimizing risk management frameworks in banking: strategies to enhance compliance and profitability amid regulatory challenges. 2021.
92. Oziri ST, Seyi-Lande OB, Arowogbadamu AAG. Dynamic tariff modeling as a predictive tool for enhancing telecom network utilization and customer experience. Iconic Res Eng Journals. 2019;2(12):436-50.
93. Oziri ST, Seyi-Lande OB, Arowogbadamu AAG. End-to-end product lifecycle management as a strategic framework for innovation in telecommunications services. Int J Multidiscip Evol Res. 2020;1(2):54-64.
94. Sanusi AN, Bayeroju OF, Nwokediegwu ZQS. Conceptual framework for building information modelling adoption in sustainable project delivery

systems. 2021.
95. Sanusi AN, Bayeroju OF, Queen Z, Nwokediegwu S. Circular economy integration in construction: conceptual framework for modular housing adoption. 2019.
96. Seyi-Lande OB, Arowogbadamu AAG, Oziri ST. Agile and Scrum-based approaches for effective management of telecommunications product portfolios and services. 2021.
97. Seyi-Lande OB, Arowogbadamu AAG, Oziri ST. A comprehensive framework for high-value analytical integration to optimize network resource allocation and strategic growth. Iconic Res Eng Journals. 2018;1(11):76-91.
98. Seyi-Lande OB, Arowogbadamu AAG, Oziri ST. Geo-marketing analytics for driving strategic retail expansion and improving market penetration in telecommunications. Int J Multidiscip Futur Dev. 2020;1(2):50-60.
99. Seyi-Lande OB, Oziri ST, Arowogbadamu AAG. Leveraging business intelligence as a catalyst for strategic decision-making in emerging telecommunications markets. Iconic Res Eng Journals. 2018;2(3):92-105.
100. Seyi-Lande OB, Oziri ST, Arowogbadamu AAG. Pricing strategy and consumer behavior interactions: analytical insights from emerging economy telecommunications sectors. Iconic Res Eng Journals. 2019;2(9):326-40.
101. Uddoh J, Ajiga D, Okare BP, Aduloju TD. AI-based threat detection systems for cloud infrastructure: architecture, challenges, and opportunities. J Front Multidiscip Res. 2021;2(2):61-7.
102. Uddoh J, Ajiga D, Okare BP, Aduloju TD. Blockchain-supported supplier compliance management frameworks for smart procurement in public and private institutions. 2021.
103. Uddoh J, Ajiga D, Okare BP, Aduloju TD. Cross-border data compliance and sovereignty: a review of policy and technical frameworks. J Front Multidiscip Res. 2021;2(2):68-74. doi: 10.54660/ijfmr.2021.2.2.68-74.
104. Uddoh J, Ajiga D, Okare BP, Aduloju TD. Cyber-resilient systems for critical infrastructure security in high-risk energy and utilities operations. 2021.
105. Uddoh J, Ajiga D, Okare BP, Aduloju TD. Designing ethical AI governance for contract management systems in international procurement frameworks. 2021.
106. Uddoh J, Ajiga D, Okare BP, Aduloju TD. Developing AI optimized digital twins for smart grid resource allocation and forecasting. J Front Multidiscip Res. 2021;2(2):55-60. doi: 10.54660/.IJFMR.2021.2.2.55-60.
107. Uddoh J, Ajiga D, Okare BP, Aduloju TD. Digital resilience benchmarking models for assessing operational stability in high-risk, compliance-driven organizations. 2021.
108. Uddoh J, Ajiga D, Okare BP, Aduloju TD. Next-generation business intelligence systems for streamlining decision cycles in government health infrastructure. J Front Multidiscip Res. 2021;2(1):303-11.
109. Uddoh J, Ajiga D, Okare BP, Aduloju TD. Streaming analytics and predictive maintenance: real-time applications in industrial manufacturing systems. J Front Multidiscip Res. 2021;2(1):285-91. doi: 10.54660/.IJFMR.2021.2.1.285-291.
110. Umar MO, Oladimeji O, Ajayi JO, Akindemowo AO, Eboseremen BO, Obuse E, *et al*. Building technical communities in low-infrastructure environments: strategies, challenges, and success metrics. Int J Multidiscip Futur Dev. 2021;2(1):51-62.
111. Umoren O, Didi PU, Balogun O, Abass OS, Akinrinoye OV. Marketing intelligence as a catalyst for business resilience and consumer behavior shifts during and after global crises. J Front Multidiscip Res. 2021;2(2):195-203.
112. Umoren O, Didi PU, Balogun O, Abass OS, Akinrinoye OV. Inclusive go-to-market strategy design for promoting sustainable consumer access and participation across socioeconomic demographics. 2021.
113. Umoren O, Didi PU, Balogun O, Abass OS, Akinrinoye OV. Integrated communication funnel optimization for awareness, engagement, and conversion across omnichannel consumer touchpoints. J Front Multidiscip Res. 2021;2(2):186-94.
114. Umoren O, Didi PU, Balogun O, Abass OS, Akinrinoye OV. Linking macroeconomic analysis to consumer behavior modeling for strategic business planning in evolving market environments. IRE Journals. 2019;3(3):203-13.